Volume 10
Number 21
7 November 2022
Pages 6053-6328

Biomaterials Science

rsc.li/biomaterials-science

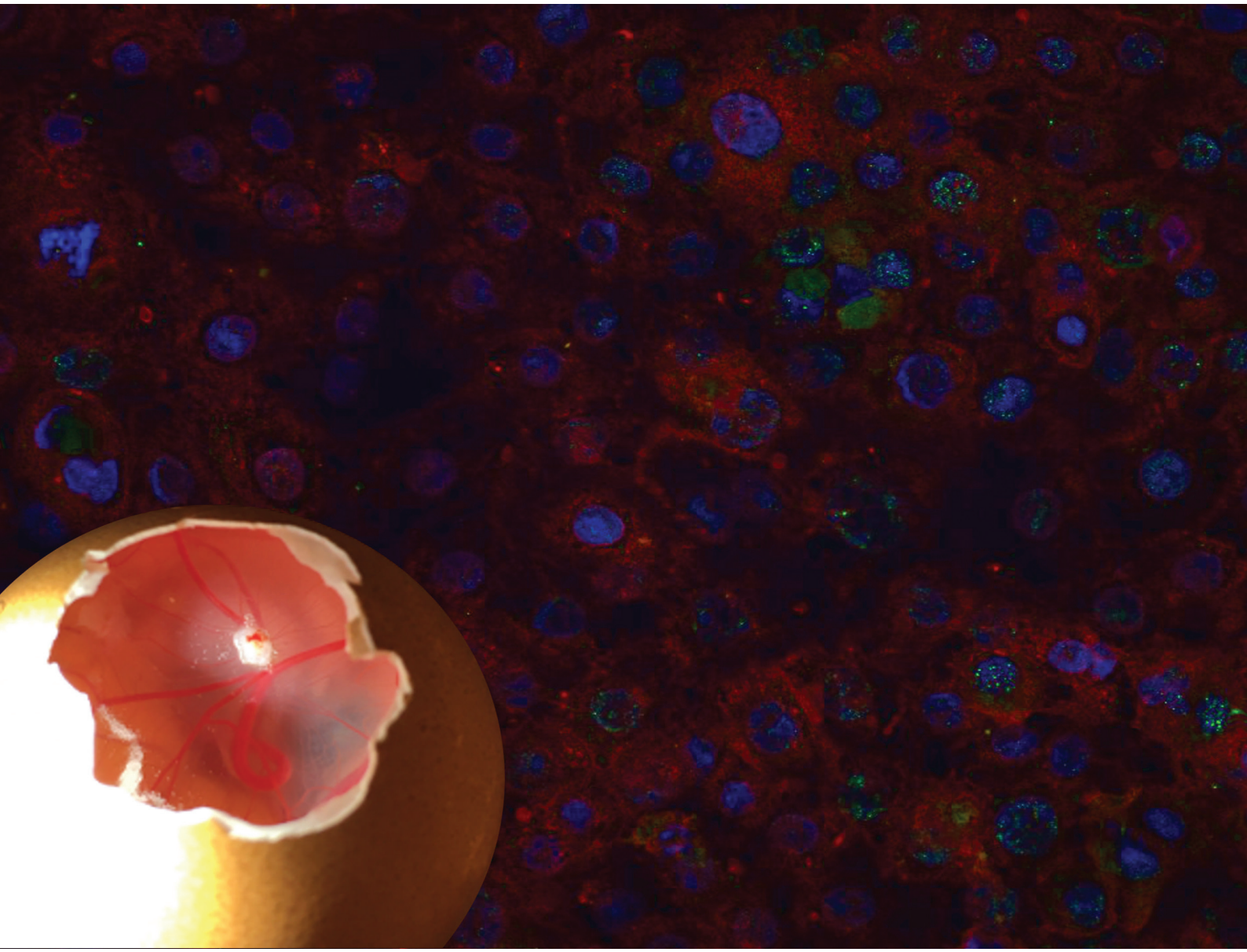

ISSN 2047-4849

ROYAL SOCIETY OF CHEMISTRY

PAPER

Valerio Voliani *et al.*

Pro-apoptotic and size-reducing effects of protein corona-modulating nano-architectures enclosing platinum prodrug in *in vivo* oral carcinoma

European Society for Biomaterials

Biomaterials Science

ROYAL SOCIETY OF CHEMISTRY

PAPER

View Article Online
View Journal | View Issue

Cite this: *Biomater. Sci.*, 2022, **10**, 6135

Pro-apoptotic and size-reducing effects of protein corona-modulating nano-architectures enclosing platinum prodrug in *in vivo* oral carcinoma†

Ana Katrina Mapanao,‡§[a] Patrizia Sarogni,§[a] Melissa Santi,§[b] Michele Menicagli,[c] Alessandra Gonnelli,[a,d] Agata Zamborlin,[a,e] Maria Laura Ermini[a] and Valerio Voliani *[a]

The selective and localized delivery of active agents to neoplasms is crucial to enhance the chemotherapeutic efficacy while reducing the associated side effects. The encapsulation of chemotherapeutics in nanoparticles decorated with targeting agents is a strategy of special interest to improve drug delivery. However, serum protein adsorption often compromises the *in vivo* efficiency of targeting agents, leading to protein corona formation that interferes with the targeting process. Here, the enhanced efficacy of hybrid nano-architectures enclosing a platinum prodrug and decorated with a customized peptide (NAs-cisPt-Tf2) is demonstrated by employing alternative *in vivo* models of oral carcinoma. The peptide binds to transferrin and modulates the protein corona formation on NAs-cisPt-Tf2, supporting the identification of its receptor. Optimized chorioallantoic membrane cancer models (CAMs) enabled a thorough assessment of the tumor-suppressing effect of NAs-cisPt-Tf2 as well as the quantitative evaluation of angiogenesis and cell cycle associated mechanisms. The treatment strategy resulted in a significant tumor volume reduction coupled with anti-angiogenic and pro-apoptotic effects inferred from the downregulation of the vascular endothelial growth factor gene and increased expression of cleaved caspase-3. Overall, this study provides a potentially effective tumor-targeted approach for a non-invasive management of oral carcinoma.

Received 27th June 2022,
Accepted 30th August 2022

DOI: 10.1039/d2bm00994c

rsc.li/biomaterials-science

1. Introduction

Chemotherapeutic agents interfere with several cellular mechanisms and target essential biomolecules for cancer cell proliferation. Chemotherapy is often combined with other standards of care for cancer management, such as surgery and radiotherapy, as a (neo)adjuvant or concomitant treatment.[1] Nonetheless, the administration of chemotherapeutics also causes toxic effects to non-malignant tissues with proliferative cells, resulting in various side effects.[2] Hence, the accurate delivery of active agents is crucial in cancer management for the reduction of adverse events to off-target organs.[3]

Molecular encapsulation in nanoparticles (NPs) is a strategy in constant development, whose ultimate goal is to provide enhanced and safer delivery of therapeutics. The improved solubility and prolonged circulation time of the molecular payloads are some of the advantages of this approach. These may lead to an increased localization of NPs in the tumor sites, also due to the enhanced permeability and retention (EPR) effect demonstrated by certain neoplasms.[4,5] The success of passive NPs-mediated drug delivery approach has been consolidated after the clinical approval of nanotherapeutics such as the liposomal formulation of doxorubicin (Doxil®/Caelyx®) and the nanoparticle albumin-bound (nab) paclitaxel (Abraxane®) for the first-line treatment of Kaposi sarcoma and metastatic breast cancer, respectively.[6] Nonetheless, the increasing demand for more efficient and safer chemotherapeutics further stimulated the development of advanced approaches for active targeting.[7,8]

Targeted therapy finds increasing clinical applications in cancer management, especially using small molecules or

[a]*Center for Nanotechnology Innovation@NEST – Istituto Italiano di Tecnologia, Piazza San Silvestro 12, 56127 Pisa, Italy. E-mail: valerio.voliani@iit.it*
[b]*NEST, Istituto Nanoscienze-CNR and Scuola Normale Superiore, Piazza San Silvestro 12, 56127 Pisa, Italy*
[c]*Fondazione Pisana per la Scienza ONLUS, via Ferruccio Giovannini 13, S. Giuliano Terme 56017, Pisa, Italy*
[d]*Radiation Oncology Unit, Pisa University Hospital, Via Roma 67, 56126 Pisa, Italy*
[e]*NEST – Scuola Normale Superiore, Piazza San Silvestro 12, 56127 Pisa, Italy*
†Electronic supplementary information (ESI) available. See DOI: **https://doi.org/10.1039/d2bm00994c**
‡Current address: Center for Radiopharmaceutical Sciences, Paul Scherrer Institute, 5232 Villigen-PSI, Switzerland.
§These authors contributed equally.

monoclonal antibodies.[9,10] It is noteworthy that both chemotherapeutic nano-encapsulation and targeted therapy have been individually implemented in clinics, while most of the systems providing their combined advantages are still at preclinical research stage.[4,6] Indeed, in physiological conditions, serum proteins are adsorbed on the surface of nanomaterials causing protein corona formation, which enables the recognition by phagocytic cells and leads to nanomaterial sequestration.[11] Likewise, protein corona formation occurs on the surface of nanomaterials decorated with targeting ligands, concealing their specificity and leading to inefficient active tumor targeting and cargo delivery.[12,13] Nevertheless, revised strategies to overcome the biological constrains have resulted in the transition of some targeted nanotherapeutics to clinical trials, with the transferrin receptor being one of the commonly targeted biomarkers.[14]

The transferrin receptor (TfR) is a transmembrane protein that enables the delivery of iron to proliferative cells, including several types of cancers wherein higher TfR expression is associated with a more aggressive phenotype.[15] Consequently, the TfR is either targeted to interfere with cancer cell proliferation and metabolism or exploited as a biomarker for selective drug delivery.[16] Therapeutic agents conjugated with TfR-recognizing ligands have been clinically evaluated for various forms of neoplasm, like liposome (SGT-53) conjugated with a transferrin (TfN) antibody fragment to deliver a plasmid encoding for wild type TP53.[17,18] However, the decoration of nanomaterials with TfN may still suffer from the masking effect of the protein corona in physiological environment, as well as from the competition with free TfN molecules for the receptor site.[19] In this regard, Santi *et al.* (2017) introduced a stealth targeting strategy using a transferrin-binding peptide (Tf2; sequence: HKYLRW) that re-modulates the protein corona composition on gold nanoparticles in serum, and efficiently binds to endogenous TfN without affecting its affinity with iron ions or TfR, or interfering with transferrin internalization.[20] This targeting approach has been integrated with hybrid nano-architectures (NAs), and the accumulation efficiency has been evaluated on multicellular spheroids of pancreatic ductal adenocarcinoma.[21] NAs are biodegradable ultrasmall-in-nano materials implemented for several oncological and antimicrobial applications.[23,25,26] These nanomaterials are rationally designed to provide advantageous medical effects as well as to avoid noble metal persistence after their intended biological action.[22,24,49]

In this work, the targeting strategy based on the protein corona-modulating Tf2 peptide is integrated with NAs containing a cisplatin prodrug (NAs-cisPt-Tf2) to improve the efficacy of the nanomaterial-mediated chemotherapy for oral carcinoma.[26] The conventional clinical use of cisplatin in treating oral cancer patients and the documented overexpression of the transferrin receptor in oral tumors further highlight the relevance of NAs-cisPt-Tf2.[27,28] Indeed, NAs-cisPt-Tf2 addresses the demand for a targeted and safe non-invasive treatment for oral cancer, in which the conservation of nearby non-malignant tissue is likewise essential.[29] Evaluations were performed on SCC-25 cells, a human papillomavirus (HPV)-negative head and neck squamous cell carcinoma (HNSCC). The usual treatment responses in HPV-negative oral cancers are notably less favorable, as documented in clinics and observed in our previous studies.[23,30] Hence, the identification of effective therapeutics for the treatment of HPV-negative tumors is pivotal. Our previous findings on the treatment of SCC-25 spheroids and tumor-grafted chorioallantoic membrane (CAM) have already demonstrated a promising antitumor response with non-targeted NAs.[31] The present study focuses on the exploitation of the TfR overexpression in oral cancer cells to specifically deliver a clinically relevant drug through nanomaterials. Treatment studies were performed on tumor-grafted chorioallantoic membrane (CAMs), a highly vascularized *in vivo* system that suitably represents the tumor and its microenvironment (TME) and compliant with the European Parliament Directive 2010/63/EU.[32] The comparison of the treatment efficacy with cisplatin and non-target NAs demonstrated an enhanced tumor volume reduction outcome together with anti-angiogenic and pro-apoptotic effects of NAs-cisPt-Tf2.

2. Methods

2.1. Nano-architectures synthesis

Nano-architectures have been produced as reported in Note 1† and characterized with standard methods (Table S1†).

2.2. 2D cell culture

Human Bronchial Epithelial cells HBEpC (Catalog No. 502-05a) were purchased from Cell Applications Inc., and human-derived squamous cell carcinoma SCC-25 (ATCC® CRL-1628™) was purchased from American Type Culture Collection (ATCC). HBEpC cells were cultured in bronchial/tracheal epithelial cell growth medium (Cell Applications 511-500) supplemented with 10% fetal bovine serum (FBS; Gibco 10500064), and SCC-25 cells were cultured in Dulbecco's Modified Eagle Medium/Nutrient Mixture F12 (DMEM/F12; Gibco 11039-021), supplemented with 10% FBS, 4 mM L-glutamine (Gibco A2916801), 1 mM sodium pyruvate (Gibco 11360070), 1× penicillin-streptomycin (equivalent to 50 U mL^{-1}; Gibco 15140-122), and 400 ng mL^{-1} of hydrocortisone (Sigma-Aldrich H0888). All indicated values correspond to the final concentrations of the supplements. The cells were maintained in an incubator set at 37 °C and 5% CO_2.

2.3. Western blot analysis for transferrin receptor expression

A pellet of cells was minced in RIPA buffer solution (Pierce™ 89901) supplemented with protease inhibitor and incubated in ice for 30 minutes. The supernatant was collected after 30 minutes of centrifugation at 14 000 rpm. Bradford assay was performed to estimate the protein concentration of the lysates using a standard calibration curve generated from the absorbance values of bovine serum albumin (BSA) solutions with different known concentrations. A volume of the lysates corresponding to 30–50 μg of proteins were mixed with gel

loading buffer, loaded in a polyacrylamide gel for SDS-PAGE, and transferred to a nitrocellulose membrane. Then, the membrane was treated with the blocking solution (1× TRIS-buffered saline with 0.1% Tween-20 and 5% powdered milk; TBST-milk) for 1 h at room temperature. Incubation of the membrane with Anti-TFRC antibody (SAB4200398 Sigma-Aldrich) for TfR and α-actin (A-3853 Sigma-Aldrich) was performed overnight at 4 °C. Following three washes in 1× TBS with 0.1% Tween-20 (TBST), the membrane was incubated with the corresponding HRP-conjugated secondary antibodies for 1 h at room temperature. After further TBST washes of the membrane, the protein bands were finally detected through enhanced chemiluminescence (ECL) kit (1705061 Biorad) and Image Quant LAS 4000 System.

2.4. Immunocytochemistry (ICC) for transferrin receptor

HBEpC and SCC-25 cells were seeded in a 24-well plate containing circular glass slides. HBEpC cells were particularly seeded on poly-L-lysine-coated glass slides (0.01% poly-L-lysine). Upon reaching about 70 to 80% confluence, the cells were fixed with 4% paraformaldehyde (PFA) for 20 minutes. After aspirating PFA, the cells were washed three times with phosphate-buffered saline (PBS; 1×) and permeabilized with 0.1% Triton-PBS for 10 minutes at room temperature. Cells were then incubated with blocking solution (5% BSA in 1× PBS) for 1 h to avoid unspecific signals. Cells can stay in the blocking solution for few weeks if stored at 4 °C. For immunocytochemical staining, the cells were incubated with Anti-TFRC antibody (SAB4200398 Sigma-Aldrich) diluted 1 : 100 in 1% BSA in PBS overnight at 4° degrees in a humid chamber. Then, the cells were washed thrice with PBS and incubated in dark with the secondary antibody conjugated with AlexaFluor-488 (diluted 1 : 100 in 1.5% BSA in PBS) for 1.5 to 2 h at room temperature. After three washes with PBS, the cells were incubated with Hoechst 33342 (Invitrogen H3570; diluted 1 : 100 in PBS) for 15 minutes and then stained with cell membrane marker CellMask® Deep Red (Invitrogen C10046; diluted 1 : 10 in PBS) for another 5 minutes at room temperature. The negative control was stained similarly except without incubation with the TfR primary antibody.

2.5. Incubation and confocal imaging of 2D cell cultures

Cells were seeded in glass-bottom Petri dish (WillCo-dish GWSt-3522) 24 hours before treatments to attach and reach 80–90% of confluence. Then, cells were treated with NAs-647-Tf2 (maximum 30 μg of nanoparticles) and incubated for 2 hours at 37 °C. Cells were washed twice with PBS and analyzed with the Olympus Fluoview 1000 (Olympus, Melville, NY) confocal microscope interfaced with a 488 nm argon laser, a 543 nm helium–neon laser, and a 633 nm diode laser. Glass-bottom Petri dishes were mounted in a temperature-controlled chamber, and all samples were viewed with a 40 × 1.42 NA oil immersion objective. All images were analyzed using ImageJ software version 1.48.

2.6. Tumor grafting on chorioallantoic membrane

Chorioallantoic membrane (CAM) tumor grafting procedure for SCC-25 has been previously optimized as reported in Sarogni *et al.*[33] Briefly, fertilized red Leghorn eggs were purchased from a local supplier and were immediately stored at 4 °C upon delivery. The eggs were placed at room temperature 1 h prior to the start of incubation, cleaned with deionized water, and placed in trays inserted in a fan-assisted incubator (FIEM MG 140/200) set at 37.5 °C with ∼47% humidity. The date of the start of incubation was assigned as embryonic day of development (EDD) 0. On EDD 3, the eggs were punctured with a small hole on the tip, which was sealed with an adhesive tape. The eggs were returned in the incubator at an upright position. Grafting was performed on EDD 6. SCC-25 cells cultured in culture plates were detached using trypsin and collected *via* centrifugation. After removing the supernatant, the cells were counted using trypan blue (Countess cell counter system). Cell suspension with known cell population was placed in another sterile 50 mL conical tube, and spun to separate and remove the supernatant. The cell pellet was then resuspended in the grafting mix composed of 1 : 1 mixture of serum-free medium and Matrigel (Corning 354234). Each egg was grafted with 2×10^6 SCC-25 cells suspended on 25 μL of grafting mix. The grafted eggs were carefully returned in the incubator.

2.7. CAM tumor treatment and monitoring

Embryo vitality and tumor engraftment were assessed pre-treatment. Once photographed using a portable digital microscope (DinoLite AM7915MZT), eggs with visible tumor masses were randomized among the treatment conditions: serum-free culture medium (control) and NAs-cisPt-Tf2. Eggs treated with NAs-cisPt-Tf2 received 0.7 mM cisplatin (∼4 μg Pt per egg). This concentration was equivalent to the administered amount of cisplatin and NAs-cisPt in the previous investigations.[26] After spinning the aliquot of NAs-cisPt-Tf2, the supernatant was removed, and the precipitate was resuspended in serum-free medium. A solution of human transferrin (holo-Transferrin, Sigma T4132-100MG) was added to the suspension, with the final TfN concentration equal to 5 μM. The suspension was incubated at 37 °C for 30 minutes on an orbital shaker to allow the binding of TfN to the Tf2 peptide to activate the NAs-cisPt-Tf2 targeting mechanism. The tumors were treated topically with 30 μL of culture medium or TfN-bound NAs-cisPt-Tf2, and then returned in the incubator.

The treated tumors were monitored and photographed on EDD 12 and 14. After taking images on EDD 14, the eggs were placed at 4 °C for at least 1 h to induce hypothermia on the chick embryo and restrict movements. The tumors were excised leaving as little membrane on the sides as possible, and stored in −80 °C for further analyses. The eggs were returned at 4 °C to euthanize the embryo. After 24 h, the organs were collected and stored at −80 °C for further analyses. Tumor dimensions were measured using a complementary software (DinoCapture 2.0). The volumes were derived

using the formula 1/2(length × width^2), where the length and width correspond to the longer and shorter measurements, respectively.[34] The data and derived measurements were further analyzed using GraphPad Prism 9, along with statistical analyses (Table S2†).

2.8. Hematoxylin and Eosin (H&E) staining

Tissues were fixed in 10% buffered formalin. Sections of 4 μm thickness were obtained from paraffin blocks using a microtome (Leica RM2255 Germany) and stained with hematoxylin–eosin (H&E). Samples were dewaxed with xylene and dehydrated with several graded ethanols and then stained with hematoxylin for 5 min (Mayer hematoxylin, Diapath C0303), stained with eosin for 1 min (Eosin G o Y alcoholic 0.5% Diapath C0353) and re-immersed in alcohol and xylene. Slides were mounted using a synthetic mounting media (Thermoscientific, LAMPB/DPX).

2.9. Immunohistochemistry

Deparaffinized samples were treated 10 min with hydrogen peroxide solution (3%) to stop peroxidase activity. Thereafter, samples immersed in EDTA-based buffer (pH 8.0) (Leica Biosystems RE7116-CE) were treated in a microwave oven (10 min, 480 W) for antigen retrieval. Nonspecific staining was prevented with blocking peptide (Abcam HRP/DAB, detection kit, ab 64261). The primary antibodies for Ki67 (rabbit monoclonal Invitrogen MA5-14520, diluted 1 : 100) and cleaved Caspase 3 (rabbit polyclonal Cell Signaling Technology, 9661; diluted 1 : 200) were applied and left overnight at 4 °C. The detection was performed using streptavidin-biotin technique (Abcam HRP/DAB, detection kit, ab 64261). Finally, the chromogen (diaminobenzidine) was used for IHC development and Mayer's hematoxylin for the counterstaining. A specific algorithm in Aperio ImageScope software (Positive Pixel Count) was used to quantitatively determine the protein expression and IHC images were processed by averaging the signal intensity of three different areas of the slide section. Therefore, a scoring system was automatically assigned to three different type of positive signal intensity, classifying them into: *weak*, *moderate* and *strong*.

2.10. Reverse Transcription – qPCR

The harvested tumors were carefully minced into pieces using a plastic pestle, and the RNA was extracted using Nucleospin RNA plus kit (MACHEREY-NAGEL 740984.50) following manufacturer's instructions. The extracted RNA samples were quantified using a nanodrop instrument (UV5NANO Mettler-Toledo), and were then immediately processed or stored at −80 °C. The quality of RNA and efficiency of the extraction procedure was confirmed through agarose gel electrophoresis, to anticipate potential problems during reverse transcription and amplification of the target gene. An aliquot of RNA extract (500 ng) was reverse transcribed for cDNA synthesis using iScript cDNA Synthesis Kit (Biorad 1708891). Then, 500 ng of total cDNA was diluted to 1 : 10 in nuclease-free water. Quantitative real-time PCR was performed with iTaq™ Universal SYBR® Green Supermix (Biorad 1725121). PCR samples were prepared with a final volume of 20 μL, with approximately 2.5 to 5 ng of cDNA template (1–2 μL cDNA). Glyceraldehyde 3-phosphate dehydrogenase (GAPDH) was used as housekeeping gene and served as loading control. The sequences of forward and reverse primers are listed in the previous study.[26] The amplification curves were visualized using SYBR Green Analysis on Applied Biosystems Instrument (7300). The recommended thermal cycling program for amplification is as follows: 95 °C for 10 minutes and 40 cycles at 95 °C for 15 seconds, 60 °C for 30 seconds and 72 °C for 30 seconds. Relative gene expression levels were calculated using $2^{-\Delta\Delta Ct}$ method.[35]

2.11. Inductively coupled plasma – mass spectrometry (ICP-MS)

An aliquot of nano-architectures was placed in a pressure vessel and dissolved in freshly prepared aqua regia (3 : 1 molar ratio of ICP-MS grade hydrochloric acid and nitric acid). For NAs-647(-Tf2) accumulation experiments on cell cultures, the same number of cells (1×10^5 cells per well) was cultured on 12-well plates, treated with nanoparticles for 2 h, washed with PBS and dissolved with aqua regia. The sealed vessels were placed in CEM Discover SP-D for further digestion under microwave irradiation at 200 °C for 15 minutes. For harvested tumors and tissues, samples were dried overnight at 80 °C until constant weight was obtained. The dried samples were transferred to pressure vessels, added with ~3 mL nitric acid, and heated up to 150 °C for 30 minutes. The acid was evaporated before another round of acid digestion with freshly made aqua regia. The samples were again heated at 150 °C for 30 minutes, until the aqua regia evaporated. The digested and dried samples were then resuspended with 3% nitric acid solution, at a final volume of 5 mL for NAS samples, and 3 mL for biological samples. The amounts of gold and/or platinum were determined after analysis on Agilent 7700 ICP-MS, using standard calibration curves.

3. Results and discussion

3.1. Overexpression of TfR in SCC-25

Transferrin receptor-mediated endocytosis has been extensively exploited to improve the internalization of clinically approved drugs or experimental anticancer compounds in the treatment of different types of carcinoma.[15] Although most oral cancer cells are known to overexpress the TfR,[28] its elevated expression in the SCC-25 line has been quantitatively identified through western blot analysis (Fig. 1A). This result, although not statistically significant, together with the immunocytochemistry staining images (Fig. 1B), confirmed the higher TfR expression in SCC-25 compared to normal epithelial cell line HBEpC. The low TfR signals (*green channel*) detected from HBEpC cells can be attributed to their proliferative potential.[36] Some TfR signals co-localized with the nuclear stain (*blue channel*), demonstrating the nuclear localization of

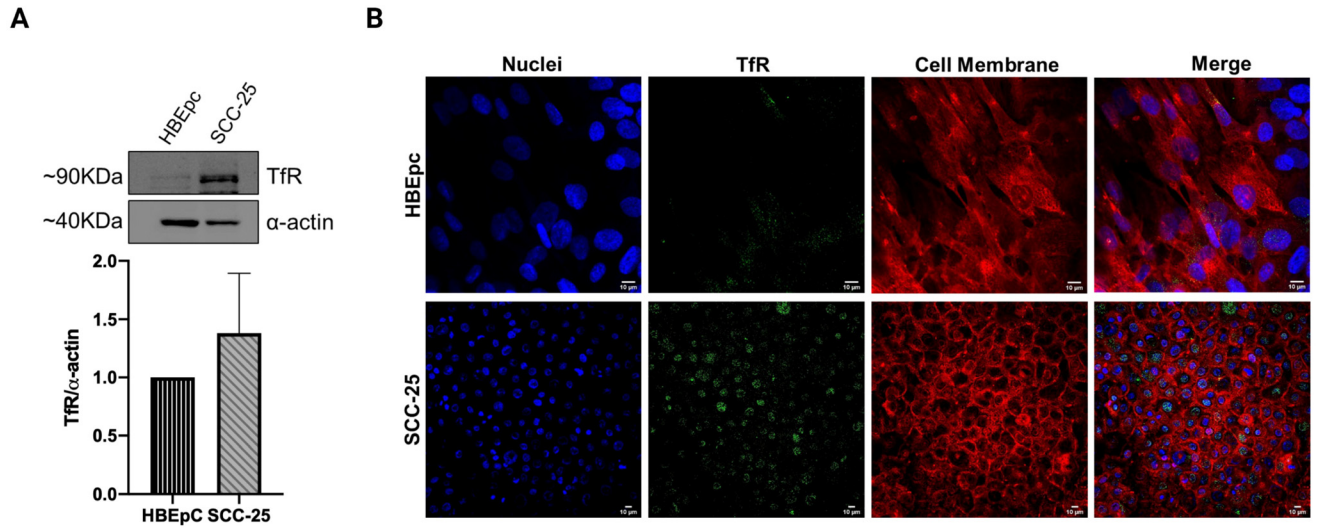

Fig. 1 Transferrin receptor (TfR) expression in SCC-25. (A) Western blot analysis demonstrating different TfR expression levels between normal cells (HBEpC) and head and neck cancer cells (SCC-25). The α-actin antibody was used to normalize the amount of proteins loaded on the gel. Densitometric analysis of the bands was performed using ImageJ, and the data is reported as the mean ± SD of two independent experiments (p-value > 0.05). (B) Representative images of immunocytochemistry staining further confirm the higher TfR signal intensity in SCC-25 cells compared to HBEpC cells. The images also depict a considerable perinuclear localization of the TfR in SCC-25 cells. Blue = Hoechst 33342 (nuclei); Green = Anti-TFRC antibody with AlexaFluor-488-conjugated secondary antibody; Red = CellMask™ Deep Red (cell membrane). Scale bars = 10 μm.

TfR in the perinuclear or juxtanuclear regions. Indeed, the transferrin ligand–receptor complex is internalized through clathrin-mediated endocytosis and delivered to the intracellular recycling endosome compartment located in proximity to the nuclei.[16,37] Overall, the biomolecular analyses confirm the suitability of TfR as a target to deliver payloads to SCC-25 and validate the active targeting strategy exploited in this study.

3.2. Preferential accumulation of Tf2 decorated NAs in SCC-25 cell cultures

In order to quantitatively investigate the internalization of the Tf2 decorated nano-architectures, NAs enclosing AlexaFluor-647 and functionalized on the surface with Tf2 peptide have been produced as previously reported (ESI Note 1†).[21,38] NAs is a group of ultrasmall-in-nano architectures with a diameter of 100–150 nm (Fig. 2A and B). The basic composition of NAs includes 3 nm gold ultrasmall nanoparticles (USNPs) coated with poly(sodium 4-styrene sulfonate) (PSS) that are electrostatically aggregated using poly(L-lysine) (PL). The average percentage of gold in NAs (quantified by inductively coupled plasma – mass spectrometry, ICP-MS) is 4.5%. The polymeric aggregates are enclosed in a silica nanoshell produced by a modified Stöber process, which also permits the subsequent surface modification. NAs surface is functionalized using a molecular linker (silane–PEG–maleimide) that enables the integration of the targeting peptide by a maleimide–thiol reaction.[21]

Cell internalization of NAs-647-Tf2 was compared with its non-functionalized counterpart (NAs-647) and was qualitatively assessed through confocal microscopy (Fig. 2C). The images demonstrated that the cells internalized both types of NAs. The signals detected from NAs-647 are attributed to passive internalization, as also observed in previous investigations.[20,21] In order to quantitatively compare the effect of the targeting strategy on the cell-internalization, a fixed amount of cells was incubated with the nano-architectures (30 μg; equivalent to ~1.5 μg of gold) with or without the Tf2 peptide modification, and the amounts of gold accumulated in the cells were measured through ICP-MS. At 2 h post-treatment, the amount of gold collected from cells treated with NAs-647-Tf2 was four times higher than the amount of gold recovered from NAs-647-treated cells (p < 0.05) (Fig. 2D). It should be noted that the NAs were delivered in serum-supplemented medium, which contains 10–15× lower concentration of TfN with respect to the physiological condition.[20,39] Nonetheless, increasing the concentration of TfN may introduce receptor-binding competition between free TfN and TfN-bound NAs-647-Tf2. In the experimental setup, the amount of TfN was not increased since the purpose of these experiments was to compare the efficiency of the receptor interaction between NAs-647 with and without Tf2.

3.3. NAs-cisPt-Tf2 efficacy on tumor-grafted chorioallantoic membrane models

The effects of NAs-cisPt-Tf2, which contains 4.5% w/w gold and 1.4% w/w platinum (%w/w = weight metal quantified by ICP-MS per weight of dried NAs), were assessed on tumor-grafted chorioallantoic membranes (CAMs) to take advantage of the reliable representation of tumors and their microenvironment, along with the presence of innate blood flow essen-

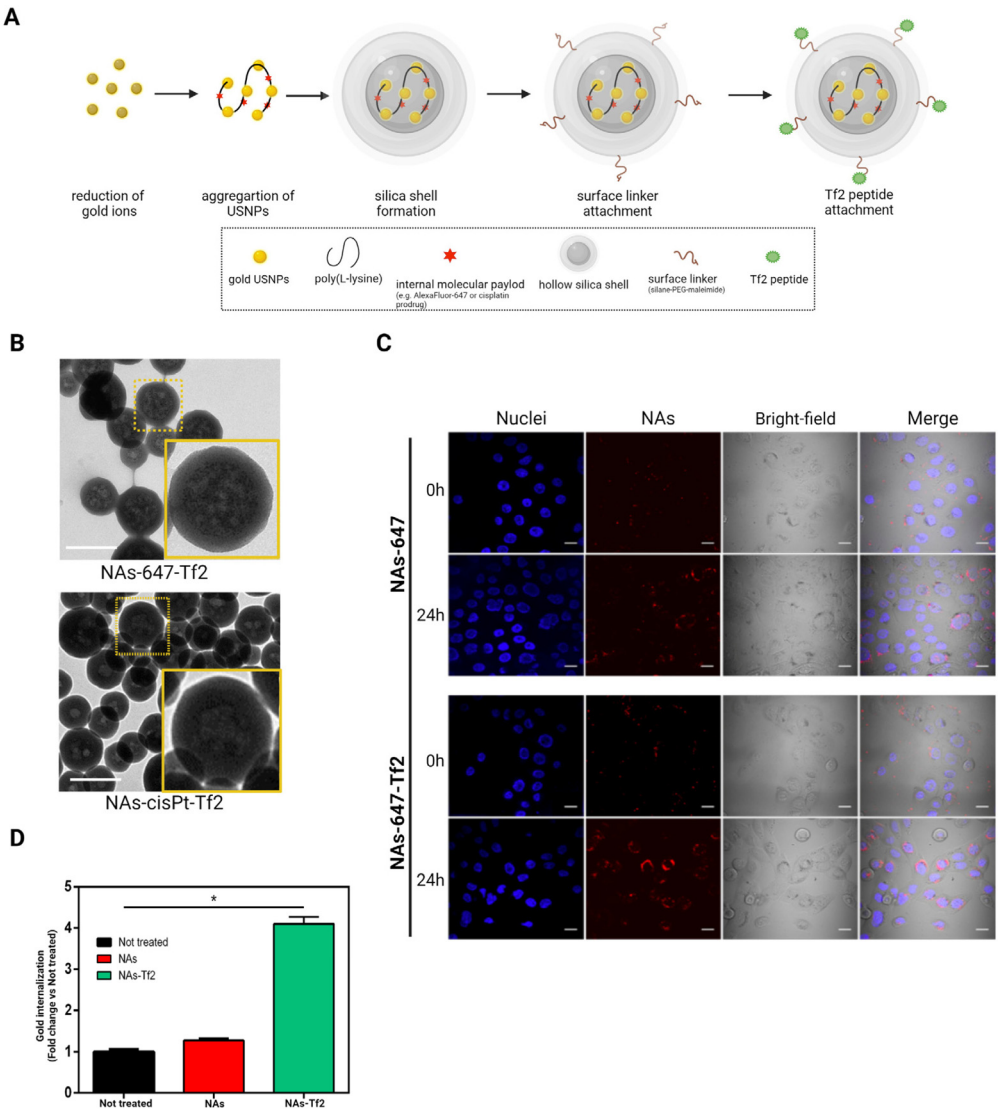

Fig. 2 Nano-architectures functionalized with transferrin-binding peptide (Tf2). (A) The scheme represents the synthesis of nano-architectures with an ultrasmall-in-nano final design. (B) Electron microscopy images show the comparable ultrasmall-in-nano design of surface-functionalized dye-containing NAs-647-Tf2 (top) and cisplatin prodrug-loaded NAs-cisPt-Tf2 (bottom); scale bars = 200 nm. (C) Confocal images illustrate the accumulation of NAs-647±Tf2 on SCC-25 cells after 2 h of incubation. The images were collected at 0 and 24 h after nanoparticles incubation. Blue = nuclei; Red = NAs-647(±Tf2); scale bars = 10 μm. (D) The amount of gold measured on cells incubated with NAs-647 or NAs-647-Tf2 was quantified and compared to the amount detected on untreated control group. The results were reported as mean ± standard deviation of $N = 3$ biological replicates. Student's t-test vs not treated. *$p < 0.05$.

tial in the targeting approach.[32] A standardized method tailored for SCC-25 neoplasms was implemented to have a consistent biological model and an effective comparison among the different treatments (Fig. 3A).[26,33] The tumor grafting procedure results in a high survival rate of the embryos, which permits the use of the system as a rough indicator of the treatment toxicity. All the treatments did not significantly affect the survival rates of the embryos on EDD 14 (Fig. S1A†).

The tumor volumes were analyzed by the measurement of their length and width (Fig. 3B, S1B, and Table S2†) to calculate the tumor fold change (Fig. S1C†).[26] The comparison between the conditions has been performed through the analysis of the relative volume fold change (R-value) (Fig. 3C and Table S3†) in order to assess the effect of the treatments regardless the differences of the initial tumor size. The tumors treated with NAs-cisPt-Tf2 have 5× smaller volumes (0.08 ± 0.06 on EDD 12 and 0.05 ± 0.02 on EDD 14) compared to the two other chemotherapy conditions (Table S4†). The enhanced therapeutic effect of NAs-cisPt-Tf2 can be attributed to the targeting strategy that elicited an increased delivery of the drug to the neoplasm, as also corroborated by the amount of platinum collected in harvested tumors (Fig. 4A). It should be noted that the administered dose (%AD) of platinum corresponds to the accumulation of the cisplatin (pro)drug at the harvesting day,

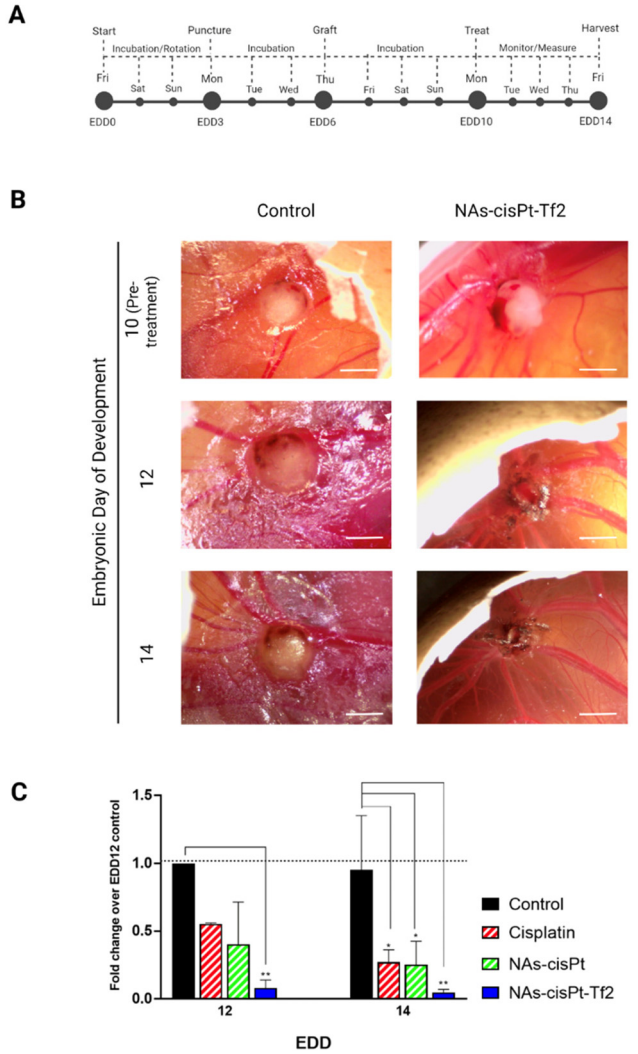

Fig. 3 Nano-chemotherapeutic evaluation on tumor-grafted CAM. (A) Previously established procedure and schedule were followed to engraft the CAMs of fertilized chicken eggs with SCC-25 cells. Tumor-grafted CAM models were randomized, treated, and monitored until EDD 14. (B) Images and measurements of tumors treated with serum-free cell culture medium (Control) or NAs-cisPt-Tf2 were taken at different time points. Scale bar = 2 mm. (C) The changes in volume of each tumor were monitored and compared to the average volume change of control tumors on EDD 12. The data are reported as mean ± standard deviation of two independent experiments, with at least 3 eggs per condition on each experiment. Statistical analysis was performed by two-way ANOVA (Tukey's multiple comparisons test) $*p < 0.05$; $**p < 0.005$. No significant differences were observed among the different type of chemotherapeutic systems ($p > 0.05$). The derivation and description of the metrics using tumor dimensions are detailed in Table S1.†

i.e. four days after the treatment. Therefore, these findings indicate that NAs-cisPt-Tf2 sustained a long-term drug accumulation compared to the untargeted NAs and the free cisplatin, even in presence of a blood flow dynamic. No significant differences were observed in the accumulation of platinum in the liver and the heart of the embryos between the conditions (Two-way ANOVA; $p > 0.1$). The gold-to-platinum mass ratio within the nano-architectures ranges between 6.1 ± 2.1. Hence, the higher %AD of gold detected in the harvested tumors treated with NAs-cisPt-Tf2 can be associated to the targeting strategy, likely the %AD trend in platinum (Fig. S1D†). This finding is of special interest for future developments towards targeted combined chemo-radiotherapy, in which the gold USNPs in NAs can act as radiosensitizers.[40]

Further biomolecular investigations were performed to identify the effects of the treatments on some cancer-related mechanisms. Vascular endothelial growth factor-A (VEGF-A), caspase-3, and proliferating cell nuclear antigen (PCNA) mRNA expressions were measured in the harvested tumors to analyze the influence of the treatment on angiogenesis, apoptotic potential, and proliferation, respectively (Fig. 4B). Consistent with the cisplatin and NAs-cisPt administration, tumors treated with NAs-cisPt-Tf2 showed a downregulation of VEGF-A mRNA expression (Fig. 4B, left) attributed to the platinum drug. On the other hand, the addition of the Tf2 peptide on NAs has slightly attenuated the downregulation of VEGF-A, probably because the transferrin itself may have a role in promoting angiogenesis.[41] For instance, Carlevaro *et al.* observed that the implantation of sponges containing transferrin of various origins (apotransferrin from human or ovotransferrin from chicken) stimulated the formation of new allantoic vessels on the CAM after 12 days of incubation.[41] It should be noted that the gold USNPs may also contribute to the VEGF-A downregulation. In this regard, Zhang *et al.* observed that gold nanoparticles stimulated the modification of the tumor microenvironment and disrupted the crosstalk between the tumor and endothelial cells in ovarian cancer.[42] Another study attributed the anti-angiogenic properties of gold nanoparticles to their selective interaction with the heparin-binding domain of VEGF and basic fibroblast growth factor (bFGF), resulting in the inhibition of VEGF signaling pathway.[43] Altogether, the VEGF-A mRNA expression results suggest that NAs-cisPt-Tf2 interferes with tumor angiogenesis.

Unexpected dynamics were observed on caspase-3 and proliferating cell nuclear antigen (PCNA) mRNA levels (Fig. 4B), wherein both were found to be upregulated in tumors treated with NAs-cisPt-Tf2. Tumor cell proliferation and apoptosis were further explored through immunohistochemistry (IHC) using anti-Ki67 and cleaved caspase-3 antibodies (Fig. 4C). IHC staining was of special interest for assessing the pro-apoptotic potential, as caspase-3 protein needs to be cleaved before proceeding with apoptosis.[44] The extent of protein expression in the IHC images were evaluated through a Positive Pixel Count algorithm in the Aperio ImageScope software (Fig. S.2†). Taken together, the IHC images and the quantitative analysis corroborate the gene expression evaluations, confirming the higher protein expression of both Ki67 and cleaved caspase-3 on tumors treated with NAs-cisPt-Tf2, although with a weak and moderate increase. Interestingly, the pro-apoptotic effect of NAs-cisPt-Tf2 differ from cisplatin and NAs-cisPt treatments, wherein the increased PCNA expression level was coupled with a caspase-3 mRNA downregulation in the untargeted treatments.[26] This behavior can be associated to both the presence

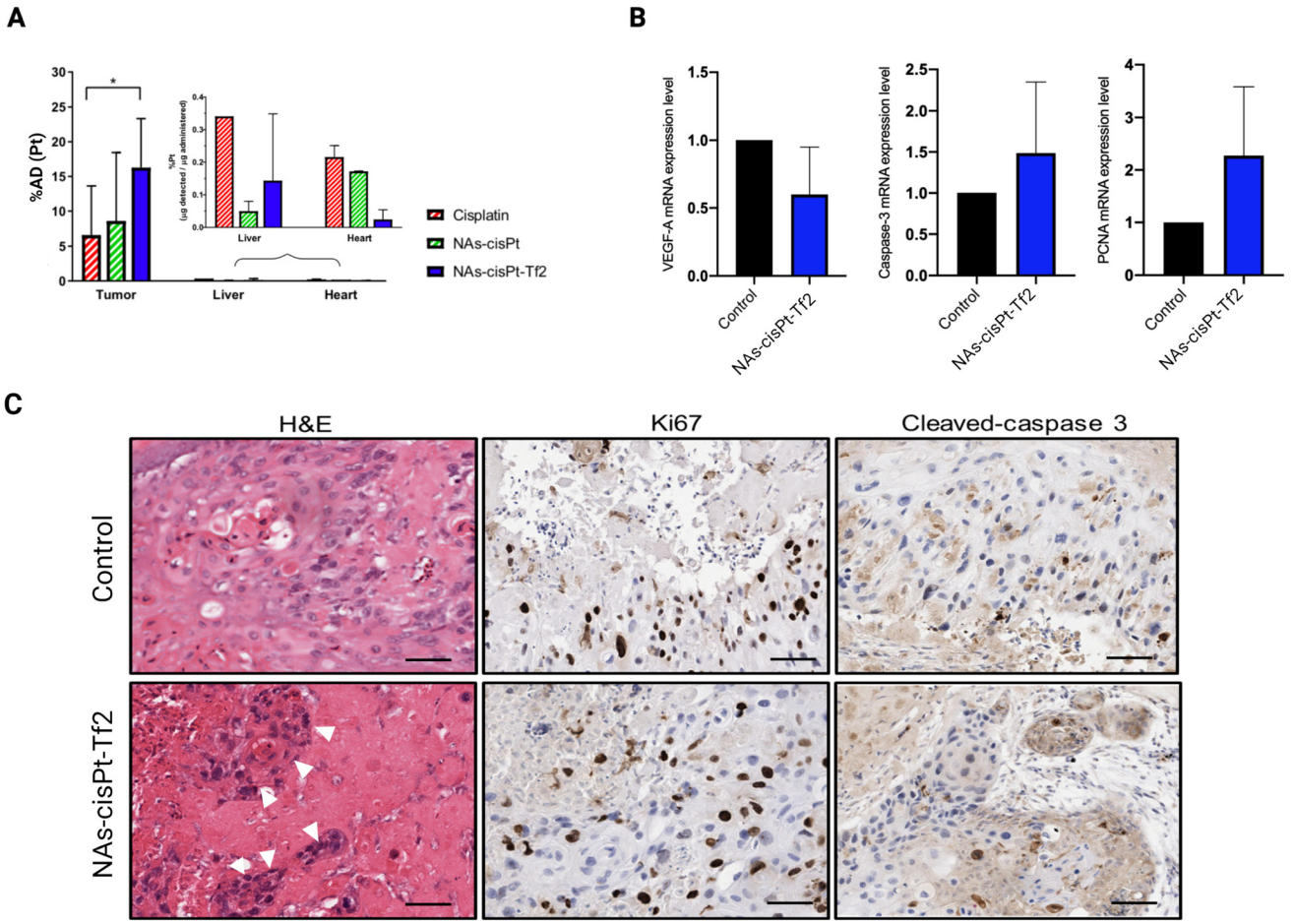

Fig. 4 Post-treatment evaluation (A) The amounts of platinum accumulated in the tumor, liver, and heart of treated models were quantified through ICP-MS. The data are reported as mean ± standard deviation and analyzed by two-way ANOVA (Tukey's multiple comparisons test) $*p < 0.05$. (B) Control and NAs-cisPt-Tf2-treated tumors were processed to identify the treatment effects on the mRNA expressions of VEGF-A (left), caspase-3 (center), and PCNA *(right)*. Statistical analysis was performed by Student's *t*-test ($p > 0.05$). (C) Hematoxylin and eosin (H&E; left) staining denoted structural damages on the tumor treated with NAs-cisPt-Tf2 compared to the control. White arrowheads indicate dispersed cell foci within the damaged area. The control and NAs-cisPt-Tf2-treated tumors were also analyzed for Ki67 (center) and cleaved-caspase 3 (right) expressions to evaluate the levels of proliferation and apoptosis, respectively. Scale bars = 200 μm.

of the targeting agent (*i.e.*, an improved accumulation of the nano-architectures in the neoplasm), and to the possible increase in intracellular iron accumulation that can lead to oxidative stress and cell death.[45–47] The elevated PCNA and Ki67 expression in the treated tumors may also be due to the tumor re-population and may indicate an increased aggressiveness of the surviving cancer cell fraction.[26,48] The contrasting implications of the upregulation of both PCNA/Ki67 and the activated form of caspase-3 demands additional investigations to clarify whether the increased apoptotic potential of the cells exceeds their propensity to proliferate, which may explain the enhanced efficacy for tumor volume reduction. Nonetheless, (neo)adjuvant treatments (*e.g.* radiotherapy) may be required to constrain the surviving cancer cells and improve the tumor management outcome.

Hematoxylin and eosin staining of the tumor samples further confirmed the morphological damages in the tumor sites caused by NAs-cisPt-Tf2. Few identifiable dispersed cellular foci were observed (Fig. 4C, left), as previously reported after treatment with unconjugated NAs.[26] Thus, the morphological impairments of the tumor masses underline the possible role of the nano-architectures in weakening the cell–cell interaction in the tumor microenvironment, which is crucial for both carcinogenesis and metastasis.

4. Conclusion

We have demonstrated that emerging nano-architectures containing a metal-based prodrug show an enhanced antitumor effect upon the conjugation with a protein corona modulating peptide. The increased accumulation of NAs-cisPt-Tf2 in comparison to its unconjugated analogue has been quantitatively confirmed on *in vitro* and *in vivo* SCC-25 oral cancer models, which resulted in an enhanced tumor volume reduction effect. Furthermore, the anti-angiogenic and pro-apoptotic effects of

NAs-cisPt-Tf2 treatment have been determined through the downregulation of VEGF-A mRNA and increased expression of the cleaved caspase-3 protein. Current endeavors are focused on the employment of the gold USNPs within NAs-cisPt-Tf2 as radiotherapy sensitizers in order to establish a platform that can elicit a localized combined action. This strategy may further constrain the remaining cancer cells after initial treatment. Investigations of additional cancer-related pathways, including genes and proteins involved in hypoxia and metastasis, may provide a more comprehensive understanding of the potential mechanisms involved in the treatment.

Notes

Data processed and graphs prepared by using GraphPad Prism software (version 8.0). The raw and processed data required to reproduce these findings are available on request to the Authors. The graphical abstract was created with BioRender.com.

Author contributions

A. K. M., M. S., P. S., cellular experiments, and data analysis; A. K. M., M. S., P. S., A. G., *in vivo* experiments, and data analysis; M. L. E., A. K. M., A. Z., nano-architectures synthesis and characterizations; M. M., histological analysis; V. V., design and coordination of the project. All Authors have discussed the data and contributed to write the manuscript.

Conflicts of interest

The authors declare no competing financial interests that could have appeared to influence the work reported in this paper.

Acknowledgements

This work was supported by the MFAG 2017 – ID 19852 from Associazione Italiana per la Ricerca sul Cancro (AIRC) granted to V. Voliani (P.I.).

References

1 E. Dickens and S. Ahmed, Principles of cancer treatment by chemotherapy, *Surgery*, 2018, **36**, 134–138, DOI: **10.1016/j.mpsur.2017.12.002**.

2 B. Shrestha, L. Tang and G. Romero, Nanoparticles–Mediated Combination Therapies for Cancer Treatment, *Adv. Ther.*, 2019, **2**, 1900076, DOI: **10.1002/adtp.201900076**.

3 E. Pérez-Herrero and A. Fernández-Medarde, Advanced targeted therapies in cancer: Drug nanocarriers, the future of chemotherapy, *Eur. J. Pharm. Biopharm.*, 2015, **93**, 52–79, DOI: **10.1016/j.ejpb.2015.03.018**.

4 A. C. Anselmo and S. Mitragotri, Nanoparticles in the clinic, *Bioeng. Transl. Med.*, 2016, **1**, 10–29, DOI: **10.1002/btm2.10003**.

5 J. Wolfram and M. Ferrari, Clinical cancer nanomedicine, *Nano Today*, 2019, **25**, 85–98, DOI: **10.1016/j.nantod.2019.02.005**.

6 A. C. Anselmo and S. Mitragotri, Nanoparticles in the clinic: An update, *Bioeng. Transl. Med.*, 2019, **4**, 1–16, DOI: **10.1002/btm2.10143**.

7 D. Bobo, K. J. Robinson, J. Islam, K. J. Thurecht and S. R. Corrie, Nanoparticle-Based Medicines: A Review of FDA-Approved Materials and Clinical Trials to Date, *Pharm. Res.*, 2016, **33**, 2373–2387, DOI: **10.1007/s11095-016-1958-5**.

8 F. Danhier, To exploit the tumor microenvironment: Since the EPR effect fails in the clinic, what is the future of nanomedicine?, *J. Controlled Release*, 2016, **244**, 108–121, DOI: **10.1016/j.jconrel.2016.11.015**.

9 A. M. Tsimberidou, Targeted therapy in cancer, *Cancer Chemother. Pharmacol.*, 2015, **76**, 1113–1132, DOI: **10.1007/s00280-015-2861-1**.

10 Y. T. Lee, Y. J. Tan and C. E. Oon, Molecular targeted therapy: Treating cancer with specificity, *Eur. J. Pharmacol.*, 2018, **834**, 188–196, DOI: **10.1016/j.ejphar.2018.07.034**.

11 E. Blanco, H. Shen and M. Ferrari, Principles of nanoparticle design for overcoming biological barriers to drug delivery, *Nat. Biotechnol.*, 2015, **33**, 941–951, DOI: **10.1038/nbt.3330**.

12 S. Tenzer, D. Docter, J. Kuharev, A. Musyanovych, V. Fetz, R. Hecht, F. Schlenk, D. Fischer, K. Kiouptsi, C. Reinhardt, K. Landfester, H. Schild, M. Maskos, S. K. Knauer and R. H. Stauber, Rapid formation of plasma protein corona critically affects nanoparticle pathophysiology, *Nat. Nanotechnol.*, 2013, **8**, 772–781, DOI: **10.1038/nnano.2013.181**.

13 P. Breznica, R. Koliqi and A. Daka, A review of the current understanding of nanoparticles protein corona composition, *Med. Pharm. Rep.*, 2020, **93**, 342–350, DOI: **10.15386/mpr-1756**.

14 R. van der Meel, L. J. C. Vehmeijer, R. J. Kok, G. Storm and E. V. B. van Gaal, Ligand-targeted particulate nanomedicines undergoing clinical evaluation: Current status, *Adv. Drug Delivery Rev.*, 2013, **65**, 1284–1298, DOI: **10.1016/j.addr.2013.08.012**.

15 S. Tortorella and T. C. Karagiannis, Transferrin receptor-mediated endocytosis: A useful target for cancer therapy, *J. Membr. Biol.*, 2014, **247**, 291–307, DOI: **10.1007/s00232-014-9637-0**.

16 T. R. Daniels, E. Bernabeu, J. A. Rodríguez, S. Patel, M. Kozman, D. A. Chiappetta, E. Holler, J. Y. Ljubimova, G. Helguera and M. L. Penichet, The transferrin receptor and the targeted delivery of therapeutic agents against cancer, *Biochim. Biophys. Acta, Gen. Subj.*, 2012, **1820**, 291–317, DOI: **10.1016/j.bbagen.2011.07.016**.

17 C. P. Leung, M. A. Barve, M.-S. Wu, K. F. Pirollo, J. F. Strauss, W.-C. Liao, S.-H. Yang, R. A. Nunan, J. Adams, J. B. Harford and E. H. Chang, *A phase II trial combining*

tumor-targeting TP53 gene therapy with gemcitabine/nab-paclitaxel as a second-line treatment for metastatic pancreatic cancer, Wolters Kluwer, 2021. DOI: 10.1200/JCO.2021.39.15_suppl.4139.

18 N. Senzer, J. Nemunaitis, D. Nemunaitis, C. Bedell, G. Edelman, M. Barve, R. Nunan, K. F. Pirollo, A. Rait and E. H. Chang, Phase I Study of a Systemically Delivered p53 Nanoparticle in Advanced Solid Tumors, *Mol. Ther.*, 2013, **21**, 1096–1103, DOI: 10.1038/mt.2013.32.

19 A. Salvati, A. S. Pitek, M. P. Monopoli, K. Prapainop, F. B. Bombelli, D. R. Hristov, P. M. Kelly, C. Åberg, E. Mahon and K. A. Dawson, Transferrin-functionalized nanoparticles lose their targeting capabilities when a biomolecule corona adsorbs on the surface., *Nat. Nanotechnol.*, 2013, **8**, 137–143, DOI: 10.1038/nnano.2012.237.

20 M. Santi, G. Maccari, P. Mereghetti, V. Voliani, S. Rocchiccioli, N. Ucciferri, S. Luin and G. Signore, Rational Design of a Transferrin-Binding Peptide Sequence Tailored to Targeted Nanoparticle Internalization, *Bioconjugate Chem.*, 2017, **28**, 471–480, DOI: 10.1021/acs.bioconjchem.6b00611.

21 A. K. Mapanao, M. Santi, P. Faraci, V. Cappello, D. Cassano and V. Voliani, Endogenously Triggerable Ultrasmall-in-Nano Architectures: Targeting Assessment on 3D Pancreatic Carcinoma Spheroids, *ACS Omega*, 2018, **3**, 11796–11801, DOI: 10.1021/acsomega.8b01719.

22 D. Cassano, A.-K. Mapanao, M. Summa, Y. Vlamidis, G. Giannone, M. Santi, E. Guzzolino, L. Pitto, L. Poliseno, R. Bertorelli and V. Voliani, Biosafety and Biokinetics of Noble Metals: The Impact of Their Chemical Nature, *ACS Appl. Bio Mater.*, 2019, **2**, 4464–4470, DOI: 10.1021/acsabm.9b00630.

23 A. K. Mapanao, M. Santi and V. Voliani, Combined chemo-photothermal treatment of three-dimensional head and neck squamous cell carcinomas by gold nano-architectures, *J. Colloid Interface Sci.*, 2021, **582**, 1003–1011, DOI: 10.1016/j.jcis.2020.08.059.

24 A. K. Mapanao, G. Giannone, M. Summa, M. L. Ermini, A. Zamborlin, M. Santi, D. Cassano, R. Bertorelli and V. Voliani, Biokinetics and clearance of inhaled gold ultrasmall-in-nano architectures, *Nanoscale Adv.*, 2020, **2**, 3815–3820, DOI: 10.1039/D0NA00521E.

25 M. Pernakov, M. L. Ermini, O. Sulaieva, D. Cassano, M. Santucci, Y. Husak, V. Korniienko, G. Giannone, A. Yusupova, I. Liubchak, M. T. Hristova, A. Savchenko, V. Holubnycha, V. Voliani and M. Pogorielov, Complementary Effect of Non-Persistent Silver Nano-Architectures and Chlorhexidine on Infected Wound Healing, *Biomedicines*, 2021, **9**, 1215, DOI: 10.3390/biomedicines9091215.

26 P. Sarogni, A. K. Mapanao, A. Gonnelli, M. L. Ermini, S. Marchetti, C. Kusmic, F. Paiar and V. Voliani, Chorioallantoic membrane tumor models highlight the effects of cisplatin compounds in oral carcinoma treatment, *iScience*, 2022, **25**, 103980, DOI: 10.1016/j.isci.2022.103980.

27 L. Q. M. Chow, Head and Neck Cancer, *N. Engl. J. Med.*, 2020, **382**, 60–72, DOI: 10.1056/NEJMra1715715.

28 T. Miyamoto, N. Tanaka, Y. Eishi and T. Amagasa, Transferrin receptor in oral tumors, *Int. J. Oral Maxillofac. Surg.*, 1994, **23**, 430–433, DOI: 10.1016/S0901-5027(05)80039-6.

29 C. L. Lazarus, J. A. Logemann, P. J. Kahrilas and B. B. Mittal, Swallow recovery in an oral cancer patient following surgery, radiotherapy, and hyperthermia, *Head Neck*, 1994, **16**, 259–265, DOI: 10.1002/hed.2880160309.

30 C. Fakhry, W. H. Westra, S. Li, A. Cmelak, J. A. Ridge, H. Pinto, A. Forastiere and M. L. Gillison, Improved survival of patients with human papillomavirus-positive head and neck squamous cell carcinoma in a prospective clinical trial, *J. Natl. Cancer Inst.*, 2008, **100**, 261–269, DOI: 10.1093/jnci/djn011.

31 M. Santi, A. K. Mapanao, D. Cassano, Y. Vlamidis, V. Cappello and V. Voliani, Endogenously-Activated Ultrasmall-in-Nano Therapeutics: Assessment on 3D Head and Neck Squamous Cell Carcinomas, *Cancers*, 2020, **12**, 1063, DOI: 10.3390/cancers12051063.

32 A. K. Mapanao, P. P. Che, P. Sarogni, P. Sminia, E. Giovannetti and V. Voliani, Tumor grafted – chick chorioallantoic membrane as an alternative model for biological cancer research and conventional/nanomaterial-based theranostics evaluation, *Expert Opin. Drug Metab. Toxicol.*, 2021, **17**, 947–968, DOI: 10.1080/17425255.2021.1879047.

33 P. Sarogni, A. K. Mapanao, S. Marchetti, C. Kusmic and V. Voliani, A Standard Protocol for the Production and Bioevaluation of Ethical In Vivo Models of HPV-Negative Head and Neck Squamous Cell Carcinoma, *ACS Pharmacol. Transl. Sci.*, 2021, **4**, 1227–1234, DOI: 10.1021/acsptsci.1c00083.

34 M. Rovithi, A. Avan, N. Funel, L. G. Leon, V. E. Gomez, T. Wurdinger, A. W. Griffioen, H. M. W. Verheul and E. Giovannetti, Development of bioluminescent chick chorioallantoic membrane (CAM) models for primary pancreatic cancer cells: A platform for drug testing, *Sci. Rep.*, 2017, **7**, 1–13, DOI: 10.1038/srep44686.

35 K. J. Livak and T. D. Schmittgen, Analysis of relative gene expression data using real-time quantitative PCR and the 2-ΔΔCT method, *Methods*, 2001, **25**, 402–408, DOI: 10.1006/meth.2001.1262.

36 P. Ponka and C. N. Lok, The transferrin receptor: role in health and disease, *Int. J. Biochem. Cell Biol.*, 1999, **31**, 1111–1137, DOI: 10.1016/S1357-2725(99)00070-9.

37 A. Nagabhushana, M. L. Chalasani, N. Jain, V. Radha, N. Rangaraj, D. Balasubramanian and G. Swarup, Regulation of endocytic trafficking of transferrin receptor by optineurin and its impairment by a glaucoma-associated mutant, *BMC Cell Biol.*, 2010, **11**, 1–19, DOI: 10.1186/1471-2121-11-4.

38 D. Cassano, M. Santi, V. Cappello, S. Luin, G. Signore and V. Voliani, Biodegradable Passion Fruit-Like Nano-Architectures as Carriers for Cisplatin Prodrug, *Part. Part. Syst. Charact.*, 2016, **33**, 818–824, DOI: 10.1002/ppsc.201600175.

39 K. Kakuta, K. Orino, S. Yamamoto and K. Watanabe, High levels of ferritin and its iron in fetal bovine serum, *Comp. Biochem. Physiol., Part A: Physiol.*, 1997, **118**, 165–169, DOI: 10.1016/S0300-9629(96)00403-3.

40 P. P. Che, A. K. Mapanao, A. Gregori, M. L. Ermini, A. Zamborlin, M. Capula, D. Ngadimin, B. J. Slotman, V. Voliani, P. Sminia and E. Giovannetti, Biodegradable Ultrasmall-in-Nano Architectures Loaded with Cisplatin Prodrug in Combination with Ionizing Radiation Induces DNA Damage and Apoptosis in Pancreatic Ductal Adenocarcinoma, *Cancers*, 2022, **14**, 3034, DOI: 10.3390/cancers14123034.

41 M. F. Carlevaro, A. Albini, D. Ribatti, C. Gentili, R. Benelli, S. Cermelli, R. Cancedda and F. D. Cancedda, Transferrin promotes endothelial cell migration and invasion: Implication in cartilage neovascularization, *J. Cell Biol.*, 1997, **136**, 1375–1384, DOI: 10.1083/jcb.136.6.1375.

42 Y. Zhang, X. Xiong, Y. Huai, A. Dey, M. N. Hossen, R. V. Roy, C. K. Elechalawar, G. Rao, R. Bhattacharya and P. Mukherjee, Gold Nanoparticles Disrupt Tumor Microenvironment - Endothelial Cell Cross Talk To Inhibit Angiogenic Phenotypes in Vitro, *Bioconjugate Chem.*, 2019, **30**, 1724–1733, DOI: 10.1021/acs.bioconjchem.9b00262.

43 P. Mukherjee, R. Bhattacharya, P. Wang, L. Wang, S. Basu, J. A. Nagy, A. Atala, D. Mukhopadhyay and S. Soker, Antiangiogenic properties of gold nanoparticles, *Clin. Cancer Res.*, 2005, **11**, 3530–3534, DOI: 10.1158/1078-0432.CCR-04-2482.

44 A. G. Porter and R. U. Jänicke, Emerging roles of caspase-3 in apoptosis, *Cell Death Differ.*, 1999, **6**, 99–104, DOI: 10.1038/sj.cdd.4400476.

45 M. Redza-Dutordoir and D. A. Averill-Bates, Activation of apoptosis signalling pathways by reactive oxygen species, *Biochim. Biophys. Acta, Mol. Cell Res.*, 2016, **1863**, 2977–2992, DOI: 10.1016/j.bbamcr.2016.09.012.

46 C. R. Reczek and N. S. Chandel, The two faces of reactive oxygen species in cancer, *Annu. Rev. Cancer Biol.*, 2017, **1**, 79–98, DOI: 10.1146/annurev-cancerbio-041916-065808.

47 D. Galaris, A. Barbouti and K. Pantopoulos, Iron homeostasis and oxidative stress: An intimate relationship, *Biochim. Biophys. Acta, Mol. Cell Res.*, 2019, **1866**, 118535, DOI: 10.1016/j.bbamcr.2019.118535.

48 L. Wang, W. Kong, B. Liu and X. Zhang, Proliferating cell nuclear antigen promotes cell proliferation and tumorigenesis by up-regulating STAT3 in non-small cell lung cancer, *Biomed. Pharmacother.*, 2018, **104**, 595–602, DOI: 10.1016/j.biopha.2018.05.071.

49 A. Zamborlin, M. L. Ermini, M. Summa, G. Giannone, V. Frusca, A. K. Mapanao, D. Debellis, R. Bertorelli and V. Voliani, The Fate of Intranasally Instilled Silver Nanoarchitectures., *Nano Lett*, 2022, **22**(13), 5269–5276, DOI: 10.1021/acs.nanolett.2c01180.